Joint Institute for Nuclear Research

Laboratory of Nuclear Problems

Final Report on the START Programme

"Modeling of radiation protection of micro-SPECT/CT components"

Supervisor:
Dr. Vladislav Rozhkov

Student:
Diego Valdés Lozada
Centro de Aplicaciones Tecnológicas y Desarrollo Nuclear, Cuba

Participation period:
October 8 - November 29
Summer Session 2025

Dubna, 2025

Contents

List of Abbreviations

SPECT : Single-Photon Emission Computed Tomography

CT : Computed Tomography

MCNPX : Monte Carlo N-Particle eXtended

ICRP : International Commission on Radiological Protection

ALARA : As Low As Reasonably Achievable

Pb : Lead

W : Tungsten

keV : kilo electron Volt

kV : kilovolt

TASMIP : Tungsten Anode Spectral Model using Interpolating Polynomials

CdTe : Cadmium Telluride

Abstract

This study employs Monte Carlo simulations using MCNPX to evaluate radiation shielding for a micro SPECT/CT scanner. The geometry, components, and materials of the imaging system were accurately modeled. Simulations were performed for SPECT using ^{99m}Tc and ^{131}I radioisotopes, and for CT using a 120 keV X-ray source with tungsten anode. Dose rates were calculated as functions of distance and lead shielding thickness (0.2-0.5 cm). Results demonstrate that low-energy ^{99m}Tc requires minimal shielding due to rapid atmospheric attenuation, while higher-energy ^{131}I and CT X-rays necessitate substantial lead shielding. The combined SPECT/CT analysis shows that a 0.4 cm Pb wall reduces safe distances to practical levels. All findings are compared against international radiation protection standards, providing guidance for optimal shielding design in hybrid imaging facilities. The methodology established provides a robust framework for radiation safety assessment in complex medical imaging environments.

1 Introduction

1.1 Main Problem and Preclinical Context

Medical imaging has revolutionized modern diagnostics, enabling non-invasive visualization of anatomical structures and physiological processes. Among these techniques, SPECT and CT play pivotal roles in contemporary medical practice. However, both modalities involve the use of ionizing radiation, necessitating rigorous safety protocols to protect patients, healthcare workers, and the public from potential harmful effects.

The fundamental challenge in hybrid imaging facilities is optimizing shielding design to minimize radiation exposure while maintaining diagnostic efficacy and operational practicality. This balance becomes particularly critical in micro SPECT/CT research settings where multiple imaging procedures may be conducted sequentially or simultaneously, potentially leading to cumulative radiation exposure for personnel conducting longitudinal studies.

1.2 Technical Background and Literature Review

SPECT provides functional information by detecting gamma rays emitted from radiopharmaceuticals administered to the patient [1], whereas CT utilizes external X-ray sources to generate high-resolution anatomical images [2]. The integration of both modalities into hybrid micro SPECT/CT systems has significantly enhanced diagnostic accuracy by precisely correlating metabolic activity with anatomical structures, creating a synergistic effect that benefits numerous clinical applications including oncology, cardiology,

and neurological disorders [3].

International regulatory bodies, such as the ICRP, have established dose limits and advocated for the ALARA principle to minimize radiation exposure [4]. Computational methods, particularly the Monte Carlo approach, have become indispensable tools for simulating radiation transport and optimizing shielding designs in complex scenarios where analytical solutions are impractical or insufficient.

1.3 Previous Research and Current Gaps

Previous studies have primarily focused on shielding evaluation for individual imaging modalities, with limited research addressing the unique challenges posed by hybrid systems. The interplay between different radiation sources (gamma emitters and X-ray tubes) in close proximity creates complex radiation fields that require comprehensive analysis. Furthermore, most existing research has concentrated on clinical-scale systems, leaving a gap in understanding regarding micro SPECT/CT scanners which present different geometric and operational considerations.

1.4 Research Objectives and Contributions

This research aims to address these gaps by providing a comprehensive shielding evaluation for a micro SPECT/CT system using advanced Monte Carlo simulations. The study characterizes dose distributions for common radioisotopes (^{99m}Tc and ^{131}I) and CT X-ray sources, evaluates the effectiveness of various lead shielding configurations, and provides practical recommendations for radiation protection in micro imaging facilities. The findings contribute to the optimization of radiation safety protocols while maintaining the operational efficiency essential for research applications.

2 Project Objectives

The primary objectives of this project were systematically designed to address key aspects of radiation shielding in hybrid imaging systems:

- To develop and validate precise Monte Carlo models of a micro-SPECT/CT scanner using MCNPX as the primary simulation tool, ensuring both geometric and physical accuracy. This foundational work will subsequently enable a comparative analysis with models developed in alternative software frameworks, such as Geant4.
- To simulate radiation transport for common SPECT radioisotopes (^{99m}Tc and ^{131}I) and CT X-ray sources across relevant energy ranges encountered in micro SPECT/CT imaging.

- To comprehensively evaluate dose rate distributions as functions of distance from radiation sources under various operational scenarios.
- To quantitatively assess the effectiveness of various lead shielding thicknesses (0.2-0.5 cm) in reducing radiation exposure to acceptable levels.
- To determine minimum safe distances for occupational workers and the public under different shielding configurations and operational modes.
- To provide evidence-based shielding recommendations compliant with international radiation safety standards while considering practical implementation constraints.

3 Work Scope

3.1 Technical Scope

This study focused on fundamental technical aspects for the evaluation of radiation shielding in hybrid imaging systems. The research was structured around the development of a detailed computational model of a micro-SPECT/CT scanner, with its geometry based on already implemented systems [5]. This modeling included the accurate representation of all major components, such as the gantry housing, the X-ray tube, the flat panel detector, the gamma camera with a pin-hole collimator, and the phantom simulating the laboratory animal, ensuring a faithful reproduction of their spatial relationships and material composition.

The core of the simulation consisted of calculating photon interactions across the energy spectra relevant to medical imaging, ranging from 20 to 180 keV. This range is critical as it covers both the gamma emissions from radioisotopes used in SPECT (such as Technetium-99m) and the X-ray spectrum generated by a Tungsten tube operating at typical diagnostic voltages for micro-CT. Accuracy at this stage was essential for realistically predicting radiation attenuation and dose deposition.

With this validated model, the study proceeded to evaluate the shielding requirements for standard laboratory configurations, simulating common operational scenarios in preclinical research facilities. The analysis specifically focused on the dose rates to which occupational staff would be exposed, considering typical work patterns and durations in these environments. The final objective was to translate these quantitative findings into practical and applicable recommendations for radiological protection. These recommendations aim for an essential balance: ensuring compliance with the strict safety limits established by regulatory bodies, without compromising the operational efficiency and logistical needs inherent to laboratory animal research.

3.2 Materials and Methods Scope

The methodological scope encompassed:

- Application of MCNPX version 2.6.0 for all radiation transport simulations
- Use of established photon cross-section libraries and physical models within the MCNPX framework
- Implementation of variance reduction techniques to ensure computational efficiency while maintaining result accuracy
- Statistical analysis of simulation results to determine confidence intervals and uncertainty estimates
- Validation of simulation approach through comparison with established radiation protection data and principles

4 Methods

4.1 Simulation Framework and Computational Approach

The radiation transport simulations in this study were performed using the MCNPX code, version 2.6.0. This software is highly regarded within the scientific community for its versatility, precision, and validated performance in simulating the transport of photons, electrons, and neutrons, making it particularly suitable for medical physics applications [6]. The selection of MCNPX was based on its comprehensive physics models, robust variance reduction capabilities, and its extensive validation in similar contexts. The simulation approach incorporated several advanced features to ensure both accuracy and computational efficiency. Detailed photon interaction physics—including the photoelectric effect, Compton scattering, and pair production—were utilized, leveraging cross-section data from the EPDL and EEDL libraries. To enhance computational efficiency for deep-penetration problems, variance reduction techniques such as exponential transformation and weight windows were implemented. For statistical reliability, each simulation tracked a sufficient number of particle histories, typically between 10^6 and 10^7, to ensure statistical uncertainties remained below 5% in regions of interest like detectors and Pb walls. Finally, energy deposition was calculated using specific tallies: the F4 tally for flux measurement in the CdTe detector with energy bins from 0.01 MeV to 2 MeV, normalized by detector volume, and the F15-F165 tallies for ambient dose calculation, which applied fluence-to-dose conversion factors to obtain a radial dose distribution from the source.

All radiation sources in this study were explicitly normalized to enable quantitative dose rate calculations. For SPECT simulations, point sources of ^{99m}Tc and ^{131}I were modeled with unit activity (10 MBq) to establish baseline dose rates, which can be linearly scaled to actual operational activities. For CT simulations, the X-ray tube was modeled operating at 100 kV with 350 μA tube current, consistent with typical micro-CT operational parameters. The dose conversion factors (FM cards: 7.86210^{10}) applied in the MCNP tallies are derived from ICRP Publication 74 fluence-to-dose conversion coefficients for photons [7], ensuring standardized dose calculations comparable to international radiation protection standards. All dose rates presented are therefore directly scalable to specific operational scenarios through linear proportionality.

4.2 Geometric Modeling and System Characterization

The geometric model implemented in MCNPX represents a micro-SPECT/CT system designed for small animal imaging, specifically for mice. This implementation exhibits remarkable detail, incorporating not only the primary imaging components but also structural elements, positioning systems, and comprehensive radiation shielding, all of which significantly influence dose distribution and protection effectiveness.

The model employs a right-handed Cartesian coordinate system where the X-axis represents the horizontal direction (positive to the right), the Y-axis the vertical direction (positive upward), and the Z-axis the scanner's axial direction (positive toward the operator), with the origin strategically located at the center of the experimental animal. The subject is modeled as a detailed mouse phantom featuring an anatomical geometry that surpasses simple approximations. The main body is an ellipsoid with a radius of 3.5 cm and a height of 1 cm, centered at the origin. Key anatomical structures include a spherical heart with a 0.25 cm radius at (0,0,0), a head modeled as a truncated cone (base radius: 1.4 cm) extending from z = -5.5 cm to -3 cm, a tail as another truncated cone (base radius: 0.3 cm) from z = 3.45 cm to 11.45 cm, and a spherical nose with a 0.15 cm radius at (0,0,-5.5). These biological materials are defined with precise elemental compositions based on ICRP data, including skin (density 1.1 g cm^{-3}) and muscle-equivalent tissue (density 1.11 g cm^{-3}). The mouse is supported by a hollow polypropylene bed, modeled as a cylinder with a total length of 45 cm (from z = -8 cm to z = 37 cm), an external radius of 2.1 cm, an internal radius of 1.9 cm, and a wall thickness of 0.2 cm.

The Computed Tomography (CT) subsystem is comprised of an X-ray tube assembly, a stainless steel box measuring 12.9 cm $\times$ 21 cm $\times$ 28 cm located between x = -24.9 cm to -12 cm. Within this assembly resides a tungsten anode modeled as an oriented parallelepiped and an inherent aluminum filtration system with a thickness of 0.11 cm and a radius of 1.5 cm positioned at x = -23 cm.

The Single-Photon Emission Computed Tomography (SPECT) subsystem includes

a detector assembly housed in a stainless steel box of dimensions 12.3 cm × 13 cm × 27.8 cm. This assembly contains a critical CdTe detector with very thin dimensions of 0.1 cm × 1.4 cm × 1.4 cm and a printed circuit board (PCB) made of Type C fiberglass measuring 0.15 cm × 8 cm × 17 cm. The entire system is enclosed within a primary gantry structure, a main cylinder made of aluminum alloy 2024 (duralumin) with an internal radius of 29.5 cm, an external radius of 30.0 cm, an axial length of 90 cm (from z = −30 cm to z = 60 cm), and a wall thickness of 0.5 cm. Additional structural components include left and right side walls and a bed support for mechanical stabilization.

Finally, a complete radiation protection shielding system is implemented via six lead walls (pure lead) forming a protective box with asymmetric thicknesses. This configuration includes a right wall (x = 33 cm to 33.3 cm, 0.3 cm thick), a left wall (x = −34 cm to −33 cm, 1.0 cm thick), along with posterior, anterior, inferior, and superior walls, each 1.0 cm thick, completing the enclosure. The 1.0 cm thickness on most walls ensures complete radiation containment, preventing any significant leakage through these boundaries. The right wall thickness was systematically varied (0.2-0.5 cm) to establish the minimum required protection for occupational safety. This approach allows for resource optimization without compromising overall shielding effectiveness, as the primary radiation directions are adequately protected by the thicker walls while the variable wall serves both protective and optimization functions.

4.2.1 Spatial Arrangement

The geometric configuration followed a typical micro SPECT/CT scanner layout with the mouse phantom at the isocenter, detectors arranged in a circular geometry, and shielding walls positioned to protect adjacent areas (Figure 1). Distances between components were based on actual system specifications to ensure practical relevance of the results.

The distances between the mouse and the components of the SPECT/CT system are shown in Figure 2.

Figure 3 shows a 3D view of the geometric arrangement.

4.2.2 Photon Attenuation Characteristics

The photon attenuation coefficients (μ) for key shielding materials were calculated using the EPDL97 photon cross-section library within MCNPX. Table 1 presents the linear attenuation coefficients for lead and air at principal energies relevant to SPECT/CT operations. These values, which are consistent with XCOM database, provide the physical basis for interpreting the observed shielding performance and atmospheric attenuation effects throughout this study.

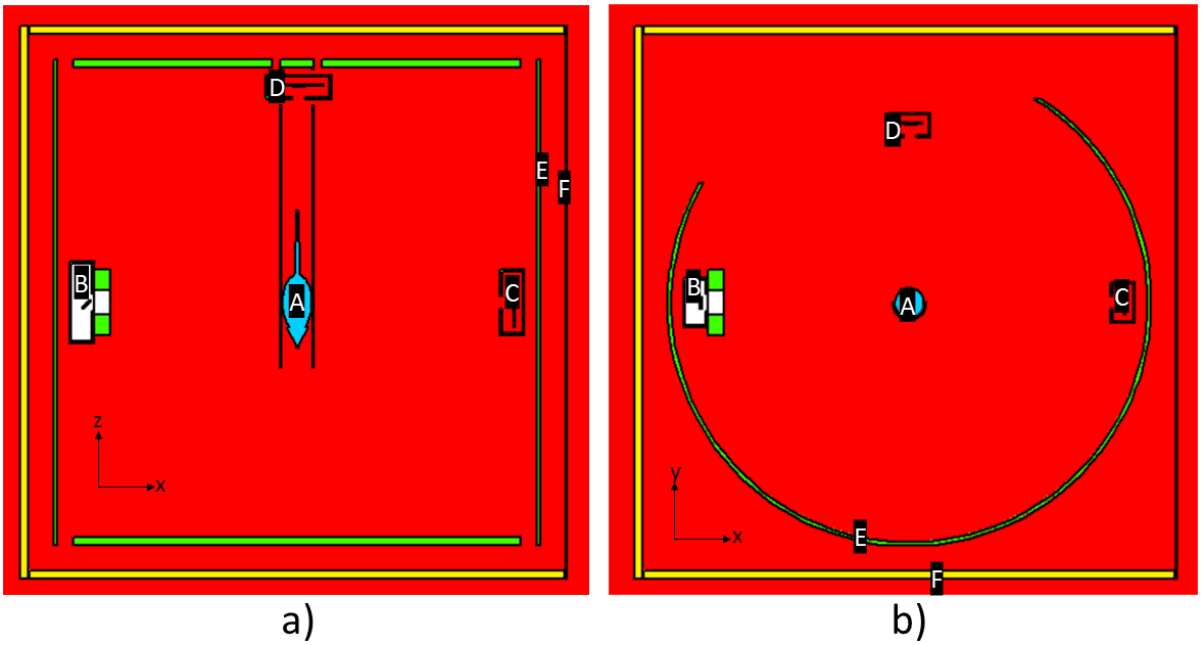

Figure 1: Schematic representation of the geometric arrangement used in the calculations: (a) xz-plane view, and (b) xy-plane view. A – mouse, B – W anode of the X-ray tube, C and D – 1 mm thick CdTe detector, E – gantry cylinder, F – Pb protective walls.

Material	140 keV (cm^{-1})	364 keV (cm^{-1})	60 keV (cm^{-1})
Lead (Pb)	28.0	5.7	56.8
Air	0.000163	0.000105	0.000185
Aluminum	0.548	0.224	0.767

Table 1: Linear attenuation coefficients (μ) for key materials at SPECT/CT relevant energies. Values calculated for Pb density = 11.35 g cm^{-3}, air density = 0.001 205 g cm^{-3}, Al density = 2.70 g cm^{-3}.

4.3 Radiation Sources and Emission Characteristics

Two distinct categories of radiation sources were simulated to represent typical micro SPECT/CT operations:

4.3.1 SPECT Radioisotopes

- ^{99m}**Tc Point Source**: Positioned at the coordinate origin (0, 0, 0) within the mouse phantom, emitting 140 keV gamma rays with 89% abundance
- ^{131}**I Point Source**: Similarly positioned, emitting multiple gamma energies with primary emissions at 364 keV (82%) and secondary emissions at 637 keV (7%) and

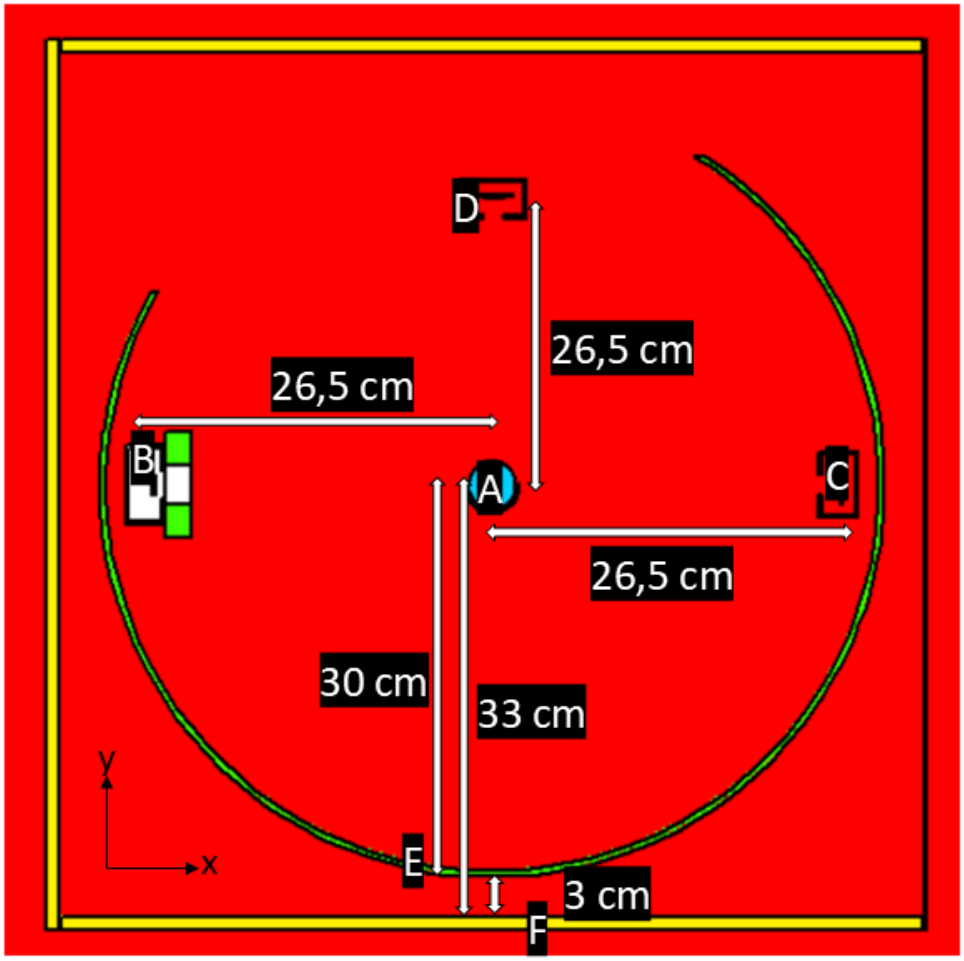

Figure 2: Distances between the mouse and SPECT/CT components, where A – mouse, B – W anode of the X-ray tube, C and D – 1 mm thick CdTe detector, E – gantry cylinder, F – Pb protective walls.

723 keV (2%)

4.3.2 CT X-ray Source

The CT simulations utilized an external X-ray tube with a tungsten anode positioned at coordinates (-25, 0, 0) and operating at 120 kV potential with 350 µA tube current, consistent with typical micro-CT operational parameters. The emission characteristics included an anode angle of 12° and inherent filtration equivalent to 2.5 mm aluminum, with beam collimation within a 20° full cone angle (10° half-angle) directed toward the phantom. The Tungsten Anode Spectral Model using Interpolating Polynomials (TASMIP) was meticulously implemented in MCNPX to generate physically accurate X-ray spectra (Figure 4) [8], with the spectral model encoded through the SDEF card using precise energy binning from 10 to 120 keV in 1 keV increments across 111 discrete energy bins that comprehensively capture both the bremsstrahlung continuum and character-

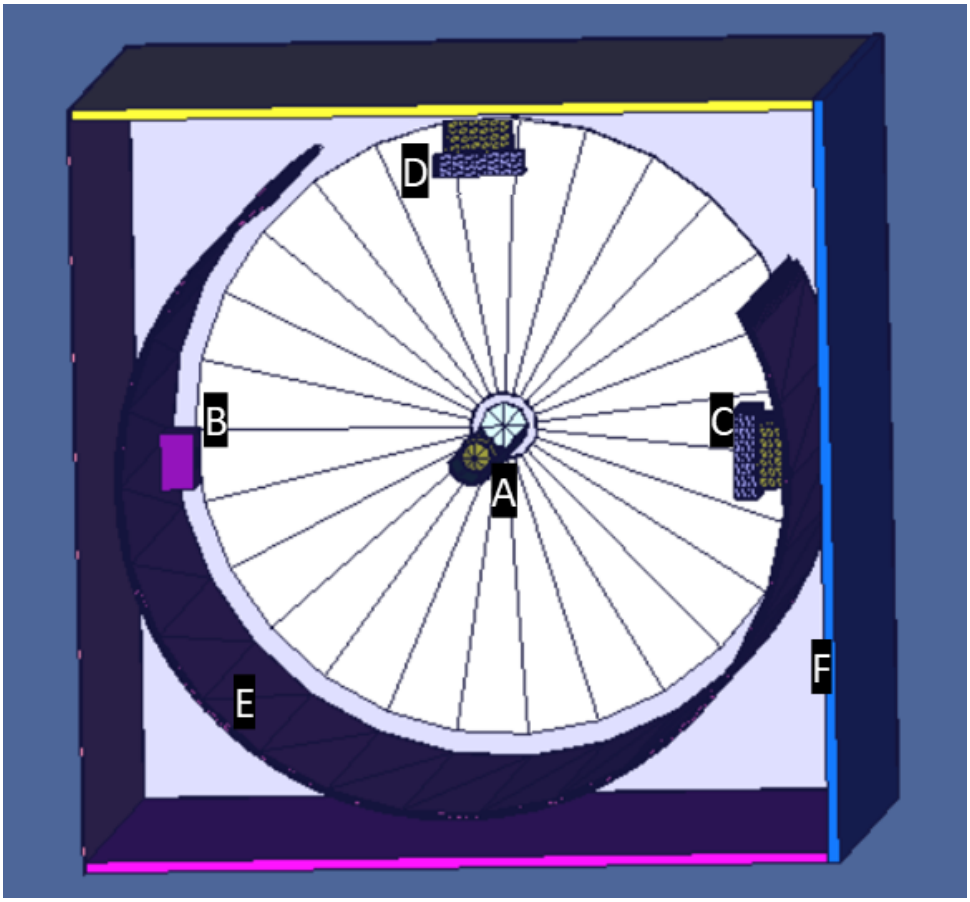

Figure 3: 3D representation of the geometric arrangement used in the calculations:A – mouse, B – W anode of the X-ray tube, C and D – 1 mm thick CdTe detector, E – gantry cylinder, F – Pb protective walls.

istic radiation emissions. The probability distribution for each energy bin was directly populated with TASMIP-calculated photon fluence values specific to the 120 kV tube potential, ensuring spectral accuracy comparable to measured X-ray tube outputs. Additional voltage variation studies were performed at 60, 70, 80, 90, 100, 110, and 120 kV to evaluate energy-dependent shielding effectiveness, with the TASMIP spectrum generated accordingly for each voltage level. This comprehensive implementation provides a rigorous computational representation of tungsten anode emission physics, enabling accurate dose calculations and shielding evaluations across the entire diagnostic energy range encountered in micro-CT imaging applications while properly accounting for spectral hardening effects and energy-dependent interactions in all radiation transport simulations.

4.4 Dose Calculation Methodology and Safety Metrics

Dose rates were calculated using an array of point detectors positioned at strategic locations ranging from 1.85 cm to 300 cm from the radiation sources (Figure 5). The calculation methodology incorporated several important aspects. Detectors were strategi-

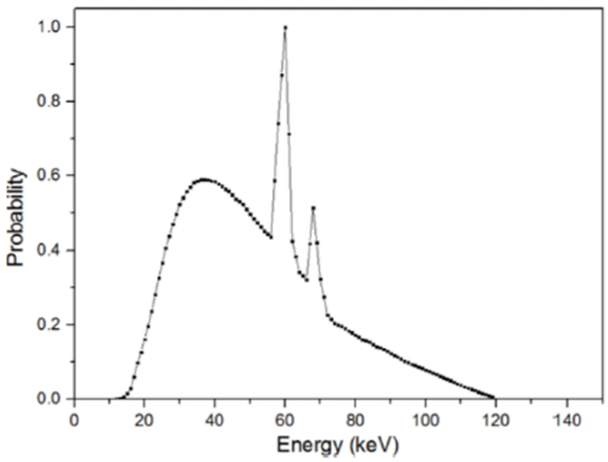

Figure 1: Figure 4: W anode spectrum for 120 kV tube potential.

cally placed at 1.85 cm, 5 cm, 10 cm, 20 cm, 30 cm, 32 cm, 33 cm, 34 cm, 35 cm, 36 cm, 38 cm, 50 cm, 60 cm, 100 cm, and 300 cm to capture both near-field and far-field dose distributions. Energy deposition tallies were converted to dose equivalent using ICRP 74 conversion coefficients for photons. The ambient dose rate limit of 2.3 µSv/h was used as the safety threshold for determining safe distances, corresponding to 1 mSv/y for occupational exposure assuming 2000 working hours annually. Additionally, statistical uncertainties were tracked for all dose calculations, with systematic uncertainties in cross-section data and geometric modeling given due consideration.

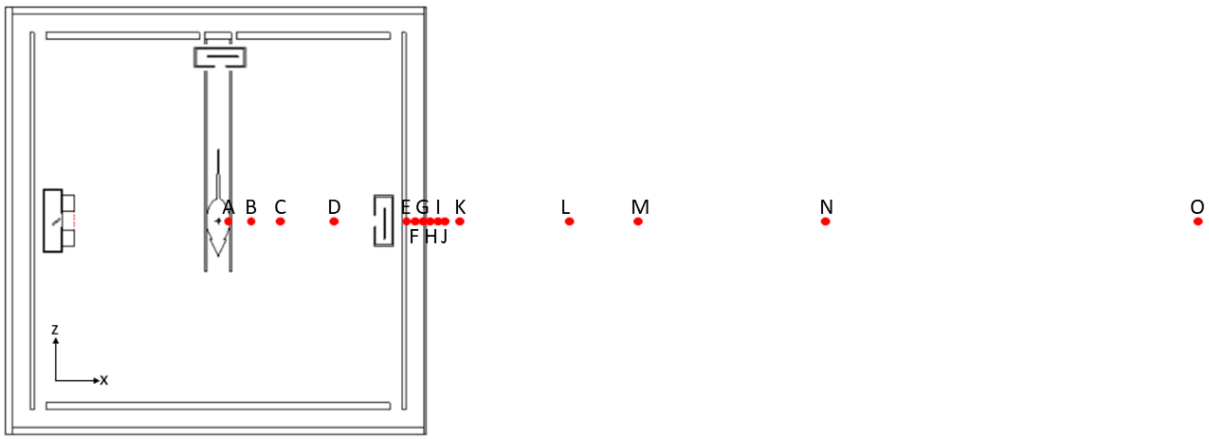

Figure 5: Red dots represent here the point detectors that are located at 1.85 cm **(A),** 5 cm**(B),** 10 cm**(C),** 20 cm**(D),** 30 cm**(E),** 32 cm**(F),** 33 cm**(G),** 34 cm**(H),** 35 cm**(I),** 36 cm**(J),** 38 cm**(K),** 50 cm**(L),** 60 cm**(M),** 100 cm**(N), and** 300 cm**(O).**

5 Results

The simulations were performed independently for both the techniques contemplated in SPECT/CT using MCNPX code. In this work we considered the dose rate behaviour for X-rays (CT simulations) as well as for radionuclides ^{99m}Tc and ^{131}I (SPECT simulations).

5.1 SPECT

Figure 6 present the plot of dose rate (mSv/h) as a function of distance (cm) for the radionuclide central to SPECT imaging: ^{99m}Tc.

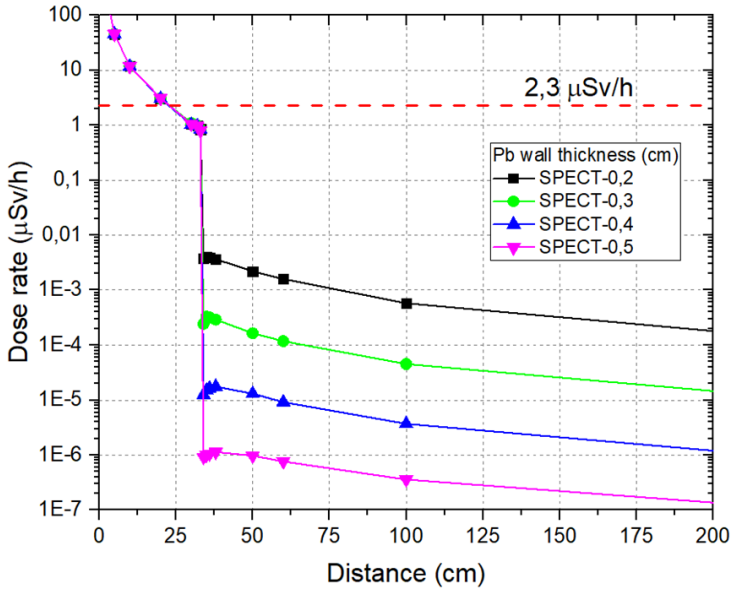

Figure 6: SPECT simulation for ^{99m}Tc radionuclide.

The simulations for ^{99m}Tc revealed distinctive radiation protection characteristics attributable to its low gamma energy (140 keV). The uncertainties associated with the dose rates for lead shielding of 0.2 cm, 0.3 cm, 0.4 cm, and 0.5 cm in thickness are 3.5%, 4.2%, 3.8%, and 4.1%, respectively. The safe distance remained remarkably constant at approximately 22.8 cm across all Pb shielding thicknesses investigated (0.2 cm to 0.5 cm) (Table 2). This consistency demonstrates that atmospheric attenuation alone provides sufficient protection for this low-energy emitter, with structural shielding offering negligible additional benefit in terms of safe distance reduction.

The dose rate profile showed rapid exponential decay with an effective attenuation coefficient of approximately 0.15 cm^{-1} in air, resulting in the dose rate falling below the 2.3 µSv h^{-1} safety threshold well before reaching the Pb shielding wall positioned at 33 cm. This behavior has important practical implications for facility design, suggesting that operational areas beyond approximately 25 cm from ^{99m}Tc sources may not require

additional structural shielding specifically for this radioisotope.

Pb (cm)	Safe Dist. (cm)	From Wall	Uncertainty
0.2	22.5	Inside gantry	±1.5 cm
0.3	22.7	Inside gantry	±1.5 cm
0.4	22.5	Inside gantry	±1.5 cm
0.5	22.8	Inside gantry	±1.5 cm

Table 2: Safe distances for each Pb thickness in SPECT simulation with ^{99m}Tc. All safe distances occur inside the gantry due to rapid atmospheric attenuation.

Since the ^{99m}Tc source decayed below 2.3 µSv/h before reaching the lead wall, an additional simulation was performed using an ^{131}I source with a lead wall thickness of 0.4 cm. The resulting dose rate is shown in Figure 7.

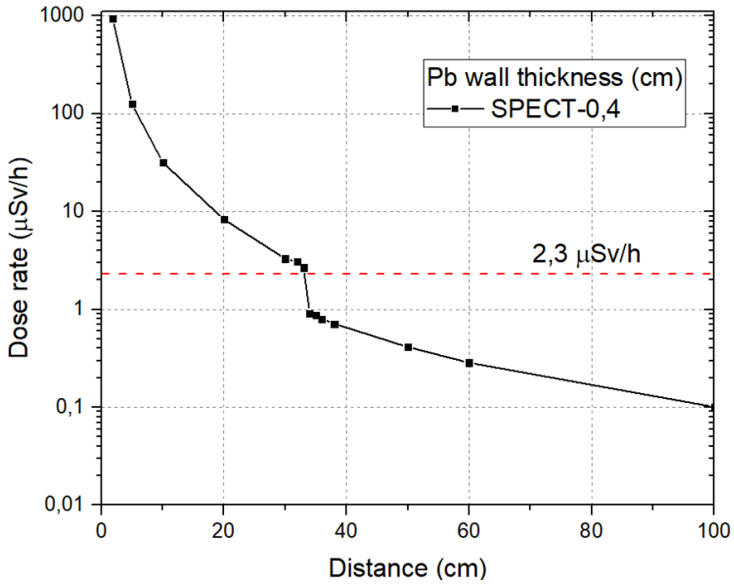

Figure 7: SPECT simulation for ^{131}I radionuclide.

In contrast to ^{99m}Tc, the ^{131}I simulations demonstrated a strong dependence on Pb shielding, with safe distances only achieved beyond the 33 cm Pb wall position resulting in an average uncertainty of 3.4%. The higher energy gamma emissions (364 keV primary) resulted in a more gradual dose rate decrease with distance, with an effective attenuation coefficient of approximately 0.08 cm^{-1} in air - nearly half that of ^{99m}Tc.

The lead shielding effectiveness for ^{131}I was quantified through the transmission factor, which decreased exponentially with shield thickness. A 0.4 cm lead wall reduced the dose rate by a factor of approximately 15 immediately after the shield, highlighting the critical role of structural shielding for medium-energy gamma emitters where atmospheric attenuation alone is insufficient for practical radiation protection.

5.2 CT

For the CT simulation, the same experimental setup used for SPECT was maintained to ensure a direct comparison. Figure 9 illustrates the resulting dose rate (μSv/h) as a function of distance from the source.

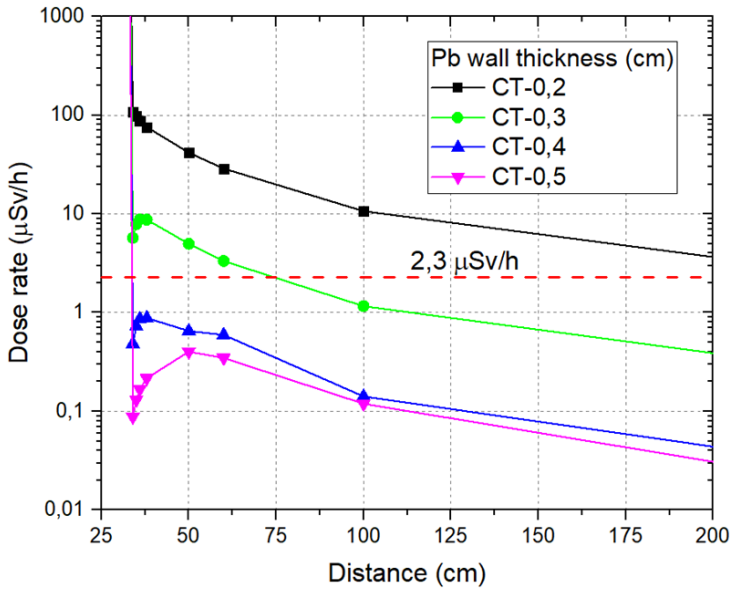

Figure 9: Dose vs distance graph for CT operating at 120 keV.

The data demonstrate that while increasing the distance from the X-ray source consistently reduces the dose rate, the presence and thickness of the Pb wall are dominant factors in achieving dose attenuation. Specifically, a thicker Pb barrier provides a significantly lower dose rate at any given distance, underscoring the critical synergy between engineered shielding (a passive safety measure) and distance (an active safety measure) in radiological protection for CT environments.

The average uncertainties in the dose rates for lead shielding with thicknesses of 0.2, 0.3, 0.4, and 0.5 cm were determined to be 0.7%, 3.2%, 3.9%, and 3.1%, respectively. These uncertainties propagate to the calculated safe distances, resulting in an estimated positional uncertainty of ±2.5 cm for distances below 50 cm and ±5.1 cm for greater distances. The evaluation of these parameters quantifies the critical importance of lead shielding for reducing the necessary safe distance, as detailed in Table 3.

Pb (cm)	Safe Dist. (cm)	From Wall (cm)	Uncertainty
0.2	243.5	210.3	±5.1 cm
0.3	74.1	40.8	±5.1 cm
0.4	33.8	0.4	±2.5 cm
0.5	33.7	0.2	±2.5 cm

Table 3: Safe distances for each Pb thickness in CT simulation.

The data reveals a dramatic, non-linear reduction in the safe distance with increasing shield thickness. The most significant protective benefit is observed with the initial addition of Pb (e.g., reducing from 0 cm to 0.3 cm), after which the returns diminish. This trend highlights that even minimal shielding is vastly superior to none, while thicker shields provide a marginal but critical extra safety buffer.

A series of simulations was conducted to quantitatively assess the shielding effectiveness of the 0.4cm lead barrier against X-rays of varying energies. The lead thickness was held constant at 0.4 cm, while the operating voltage of the X-ray tube was systematically varied across a clinical range of 60, 70, 80, 90, 100, 110, and 120 kV. This methodology was designed to evaluate the energy-dependent penetration power of the bremsstrahlung photons through the protective shielding.

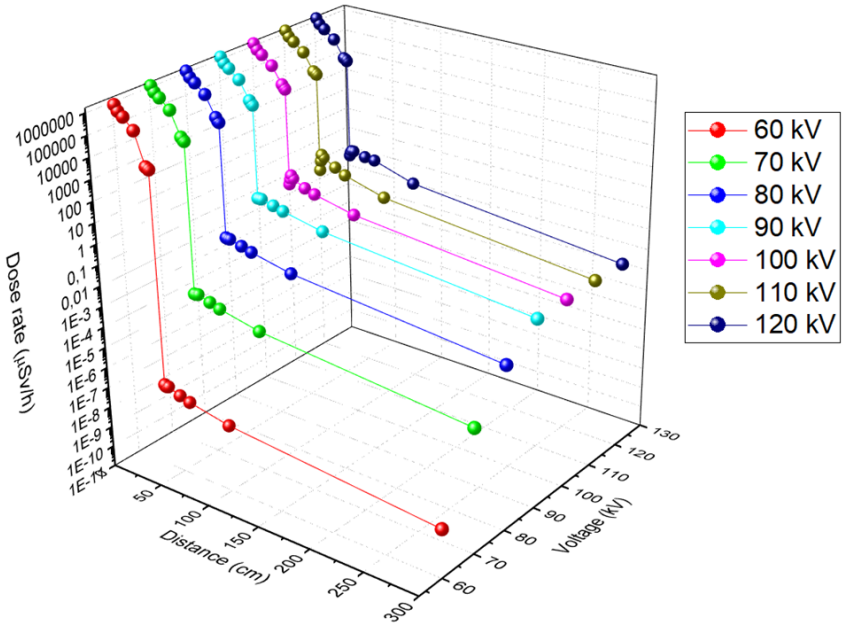

Figure 10: Dose rate vs distance for CT operating at different voltages (60-120 kV) with a Pb wall thickness of 0.4 cm.

The results, summarized in Figure 10, demonstrate a clear and positive correlation between the incident photon energy (governed by the tube voltage) and the penetrating capability of the radiation. The average uncertainties associated with the dose rates for tube voltages of 60, 70, 80, 90, 100, 110, and 120 kV are 0.8%, 1.2%, 3.5%, 4.9%, 5.1%, 4.1%, and 3.9%, respectively. Spectra generated at higher tube voltages (e.g., 120 kV) exhibited significantly higher transmission through the Pb shield compared to those generated at lower voltages (e.g., 60 kV). This is directly evidenced by the elevated dose rates measured beyond the shielding for higher energies. Consequently, the attenuation provided by a fixed thickness of Pb is less effective for higher-energy X-ray spectra, underscoring the critical need to account for the maximum operating energy when designing

radiation protection for CT components.

5.3 SPECT/CT

Given that both radiation sources (X-rays and ^{99m}Tc) emit photons, their dose rates are additive. This allows for the calculation of the total dose rate at any given point. Figure 11 shows the total dose rate as a function of distance.

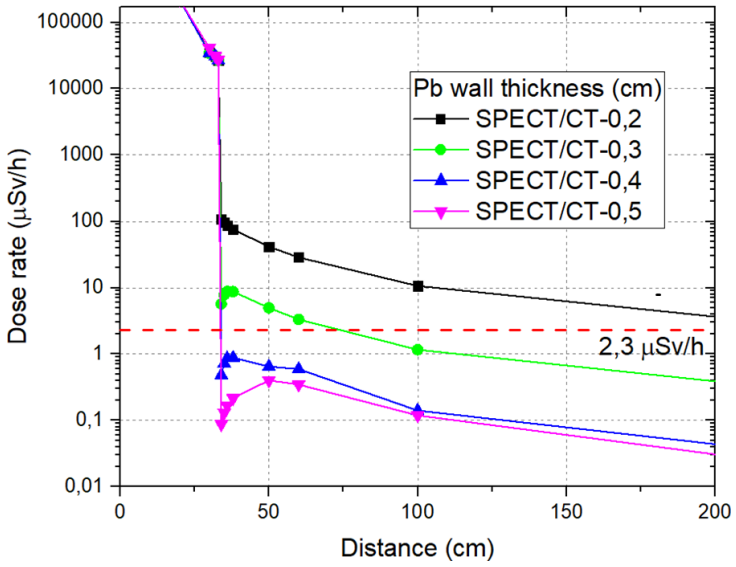

Figure 11: Dose rate vs. distance for the combined SPECT/CT study of ^{99m}Tc and X-rays at lead wall thicknesses of 0.2, 0.3, 0.4, and 0.5 cm. The red dashed line indicates the ambient dose rate of 2.3 µSv/h.

For combined operations using ^{99m}Tc with CT, the safe distances closely mirrored those of CT alone across all shielding configurations. The ^{99m}Tc contribution to the total dose rate became negligible beyond approximately 30 cm due to rapid atmospheric attenuation, resulting in the CT component dominating the combined dose rate profile. This indicates that shielding design for facilities using ^{99m}Tc micro SPECT/CT systems can primarily focus on CT protection requirements. The uncertainties associated with two distinct measurement sets are combined under the assumption of independence by applying the root sum square (RSS) method. This approach, provides a realistic estimate of the total uncertainty when there is no known correlation between the errors of the different datasets. The resulting combined uncertainties for the analyzed value pairs are 3.57%, 5.28%, 5.45%, and 5.14%, for 0.2 cm, 0.3 cm, 0.4 cm and 0.5 cm, respectively.

The same procedure was applied to the ^{131}I source in the combined SPECT/CT setup. Figure 12 shows that the dose rate falls below the ambient level at a distance of 33.9 cm from the mouse, which is 0.5 cm after the photons pass through the lead wall.

The combined analysis for ^{131}I with CT operations revealed a more complex interac-

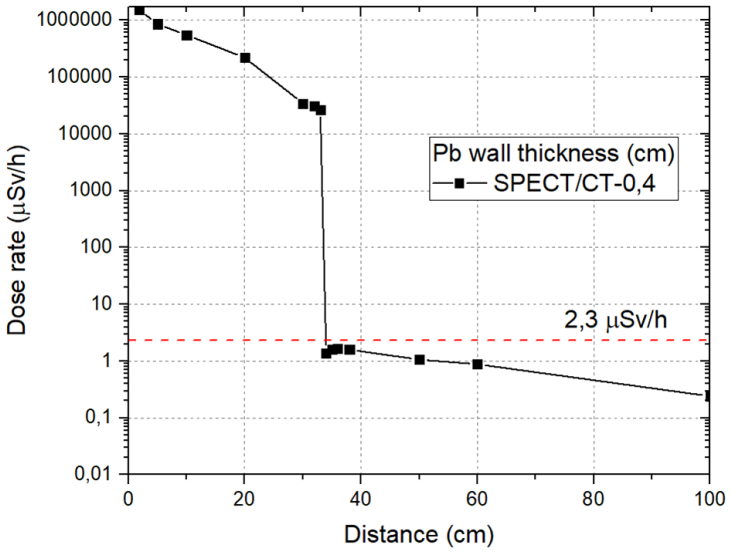

Figure 12: Dose rate vs. distance for the combined SPECT/CT study of ^{131}I and X-rays at a lead wall thickness of 0.4 cm. The red dashed line indicates the ambient dose rate of 2.3 µSv/h.

tion between the two radiation sources. With a 0.4 cm Pb wall, the dose rate fell below the safety threshold at 33.9 cm from the mouse phantom, just 0.5 cm beyond the shielding wall, resulting in an average uncertainty of 5.2%. The ^{131}I contribution remained significant at this distance due to its higher energy gamma emissions, requiring consideration of both sources in protection planning.

The results emphasize that for higher-energy SPECT radioisotopes like ^{131}I, both sources contribute meaningfully to the total dose rate, necessitating comprehensive shielding design that addresses the characteristics of all significant radiation sources in the facility.

6 Conclusion

6.1 Discussion of Key Findings

This study successfully demonstrated the application of advanced Monte Carlo methods for comprehensive shielding evaluation in hybrid imaging systems. The results reveal several fundamental principles with important implications for radiation protection in micro SPECT/CT imaging facilities:

6.1.1 Energy-Dependent Protection Requirements

The research clearly demonstrates the energy-dependent nature of radiation protection requirements. Low-energy emitters like ^{99m}Tc (140 keV) benefit significantly from at-

mospheric attenuation, requiring minimal structural shielding for personnel protection. In contrast, higher-energy sources including ^{131}I (364 keV) and CT X-rays (up to 120 keV) necessitate substantial engineered shielding, as distance alone provides insufficient protection within practical facility dimensions.

6.1.2 Shielding Optimization and Diminishing Returns

The relationship between lead thickness and protection effectiveness follows a strongly nonlinear pattern, with the most substantial benefits achieved with initial shielding additions. The shielding design was optimized through systematic evaluation of various Pb thicknesses, identifying 0.4 cm as the optimal protection thickness. The dramatic reduction in safe distance achieved with minimal lead shielding underscores the cost-effectiveness of engineered shielding compared to relying solely on distance-based protection. However, the diminishing returns at greater thicknesses suggest practical optimization limits for most applications.

6.1.3 Hybrid System Considerations

The combined micro SPECT/CT analysis confirms that shielding requirements in hybrid systems are typically dominated by the higher-energy component, which for most practical scenarios is the CT X-ray source. However, for systems utilizing higher-energy SPECT radioisotopes like ^{131}I, both sources contribute significantly to total dose rates, requiring comprehensive protection strategies.

6.2 Concluding Remarks

This research has established a comprehensive framework for evaluating radiation shielding in micro SPECT/CT systems using advanced Monte Carlo methods. The findings provide practical guidance for facility design and operation while contributing to the fundamental understanding of radiation protection in hybrid imaging environments. The methodology and results form a solid foundation for ongoing optimization of radiation safety in increasingly complex medical imaging applications, ensuring that diagnostic and research benefits can be realized while maintaining the highest standards of personnel and public protection.

The successful application of this approach demonstrates the powerful role of computational methods in addressing complex radiation protection challenges, highlighting the continued importance of physics-based approaches in advancing medical imaging safety and efficacy.

7 References

References

[1] S. B. Hansen and D. Bender, Advancement in Production of Radiotracers, Seminars in Nuclear Medicine, vol. 52, no. 4, pp. 266–275, Jul. 2022. DOI: [https://doi.org/10.1053/j.semnuclmed.2021.10.003].

[2] Willi A. Kalender, X-ray computed tomography, Physics in Medicine and Biology, vol. 51, no. 13, pp. R29–R43, Jun. 2006. DOI: https://doi.org/10.1088/0031-9155/51/13/R03.

[3] Giuliano Mariani, Laura Bruselli, Torsten Kuwert, Edmund E. Kim, Albert Flotats, Ora Israel, Maurizio Dondi y Naoyuki Watanabe, A review on the clinical uses of SPECT/CT, European Journal of Nuclear Medicine and Molecular Imaging, vol. 37, no. 9, pp. 1959–1985, 2010. DOI: https://doi.org/10.1007/s00259-010-1390-8

[4] International Commission on Radiological Protection. ICRP Statement on Tissue Reactions. ICRP Publication 118, 2017.

[5] L. Cao, T. Kriesche, W. Semmler, and J. Peter, Geometric Co-Calibration of an Integrated Small Animal SPECT-CT System for Intrinsically Co-Registered Imaging, *IEEE Transactions on Nuclear Science*, vol. 56, no. 5, pp. 2759–2767, Oct. 2009. DOI:https://doi.org/10.1109/TNS.2009.2025589

[6] Waters LS, McKinney GW, Durkee JW, et al. The MCNPX Monte Carlo Radiation Transport Code. AIP Conference Proceedings, 2007; 896(1): 81. DOI: https://doi.org/10.1063/1.2720459.

[7] International Commission on Radiological Protection, Conversion Coefficients for Radiological Protection Quantities for External Radiation Exposures, Annals of the ICRP, vol. 40, no. 2-5, pp. 1-114, 2010. DOI: https://doi.org/10.1016/j.icrp.2011.10.001.

[8] Sisniega, A., Desco, M., and Vaquero, J. J., Modification of the TASMIP x-ray spectral model for the simulation of microfocus x-ray sources, Medical Physics, vol. 41, no. 1, p. 011902, 2014. DOI: http://dx.doi.org/10.1118/1.4837220

8 Acknowledgments

I would like to express my sincere gratitude to my supervisor, Dr. Vladislav Rozhkov, for his invaluable guidance, mentorship, and support throughout this research project.

I also extend my profound appreciation to the Joint Institute for Nuclear Research for providing the exceptional resources, facilities, and intellectual environment necessary for this work. This research was conducted under the START Programme, and I am deeply thankful for this exceptional opportunity for professional development and international scientific collaboration.